AIAA 2003-3589
Transition in a Supersonic Boundary-Layer Due to Roughness and Acoustic Disturbances

P. Balakumar
NASA Langley Research Center
Hampton, VA

33rd Fluid Dynamics Conference
23–26 June 2003
Orlando, FL

TRANSITION IN A SUPERSONIC BOUNDARY-LAYER DUE TO ROUGHNESS AND ACOUSTIC DISTURBANCES

P.Balakumar
Flow Physics and Control Branch
NASA Langley Research Center, Hampton, VA 23681

Abstract

The transition process induced by the interaction of an isolated roughness with acoustic disturbances in the free stream is numerically investigated for a boundary layer over a flat plate with a blunted leading edge at a free stream Mach number of 3.5. The roughness is assumed to be of Gaussian shape and the acoustic disturbances are introduced as boundary condition at the outer field. The governing equations are solved using the 5th-order accurate weighted essentially non-oscillatory (WENO) scheme for space discretization and using third-order total-variation-diminishing (TVD) Runge-Kutta scheme for time integration. The steady field induced by the two and three-dimensional roughness is also computed. The flow field induced by two-dimensional roughness exhibits different characteristics depending on the roughness heights. At small roughness heights the flow passes smoothly over the roughness, at moderate heights the flow separates downstream of the roughness and at larger roughness heights the flow separates upstream and downstream of the roughness. Computations also show that disturbances inside the boundary layer is due to the direct interaction of the acoustic waves and isolated roughness plays a minor role in generating instability waves.

Introduction

Transition from laminar to turbulent state in shear flows occurs due to evolution and interaction of different disturbances inside the shear layer. Though there are several mechanisms and routes to go from a laminar to a turbulent state, all of them generally follow these fundamental processes:

- Receptivity
- Linear instability
- Nonlinear instability and saturation
- Secondary instability and breakdown to turbulence

In the receptivity process, the unsteady disturbances in the environments such as acoustic and turbulence interact with the inhomogeneities in the geometry such as roughness and generate instability waves inside the shear layer. In quiet environments, the initial amplitudes of these instability waves are small compared to any characteristic velocity and length scales in the flow. In the second stage, the amplitudes of these instability waves grow exponentially downstream and this process is governed by the linearized Navier-Stokes equation. Further downstream, the amplitudes of the disturbances become large and the nonlinear effects inhibit the exponential growth and the amplitude of the waves eventually saturate. In the next stage, this finite amplitude saturated disturbances become unstable to two- and/or three-dimensional disturbances. This is called secondary instability and beyond this stage the spectrum broadens, due to complex interactions and further instabilities, and the flow becomes turbulent in a short distance downstream. In this paper, the receptivity process induced by an isolated roughness and acoustic disturbances in a supersonic boundary layer with a free stream Mach number of 3.5 is investigated.

Predicting transition onset and transition end points accurately, modeling this transitional region and modeling the turbulence region are the major difficulties in computing the aerodynamic quantities accurately using the CFD codes. Our understanding of different

instability mechanisms and of different transition processes in shear layers have greatly improved in the last several decades. However the transition prediction methods have not made much progress. The main difficulty is due to the nature of the transition process itself. The transition process mainly depends on the boundary layer characteristics and on the frequency and wave number distributions of the disturbances that enter the boundary layer. The laminar boundary layer profiles can be computed easily. The problem is computing, predicting or prescribing the initial spectral, amplitude and phase, distribution of the disturbances inside the boundary layer. As we discussed earlier, the initial disturbances are generated by the interaction of the free stream unsteady disturbances and the roughness on the surface. These two are stochastic in nature and are difficult to quantify in general. In any new transition prediction strategy, one should quantify these two quantities and should determine what is the minimum amount of information necessary to predict the transition onset accurately. The objectives of this research work are to answer some of these questions and eventually to come up with an improved transition prediction method.

There are numerous investigations conducted on the interaction of acoustic waves with supersonic boundary layers. Mack (1976), Gapanov (1977) investigated the interaction of acoustic waves with a supersonic boundary layer at finite incident angles using inhomogeneous stability equations. One important finding was that due to the interaction, the acoustic waves excite disturbances inside the boundary layer, which are much larger than that in the free stream. Gapanov and Smorodsky (1999) studied the interaction of streamwise acoustic waves with a non-parallel boundary layer. The analysis and the calculations showed that the disturbances inside the boundary layer reach significant values compared to that in the outside. It was also observed that there exists a critical Reynolds number where this excitation is the highest. Fedorov and Khokhlov (1991) investigated using asymptotic theory the excitation of first and second modes by the acoustic waves near the leading edge region. Gapanov (1993) showed that the energy is transmitted to the T-S waves near the critical region where the ratio between the reflected waves and the incident wave is the largest. There are not many numerical calculations performed to investigate the interaction of acoustic waves with a flat plate including bluntness. Since there are forced disturbances and the modal disturbances what are the relative magnitudes of them and how far the forced disturbances persist are not very well understood.

There were several transition experiments performed at NASA Langley in the Mach 3.5 Supersonic Low-Disturbance tunnel. Boundary-layer transition data on a flat plate and on a cone, and free stream noise levels and the power spectral distribution of the free stream noise are presented in Chen et. al (1988). As a first step, the computations are performed for the same conditions as in the experiment. An isolated two and three-dimensional Gaussian shaped roughness is placed near the neutral stability region and the steady flow field induced by them are investigated. Secondly the interaction of the two dimensional acoustic disturbance with a blunted semi-infinite plate with and without two-dimensional roughness element located near the neutral point are investigated to identify the effect of acoustic incident angle and the roughness in receptivity process in a supersonic boundary layer. A schematic diagram of the computational set up is depicted in figure 1.

Governing Equations.

The equations solved are the three-dimensional unsteady compressible Navier-Stokes equations in conservation form

$$\frac{\partial}{\partial t} Q_i + \frac{\partial}{\partial x_j}\left(F_{ji} - F_{vji}\right) = 0.$$

$$\text{Here} \quad Q_i = \begin{Bmatrix} \rho \\ \rho E \\ \rho u \\ \rho v \\ \rho w \end{Bmatrix} \qquad \left[F_{ji}\right] = \begin{Bmatrix} \rho u_j \\ (\rho E + p)u_j \\ \rho u u_j + \delta_{1j} p \\ \rho v u_j + \delta_{2j} p \\ \rho w u_j + \delta_{3j} p \end{Bmatrix}$$

$$\left[F_{vij}\right] = \begin{Bmatrix} 0 \\ u\tau_{1j} + v\tau_{2j} + w\tau_{3j} - q_j \\ \tau_{1j} \\ \tau_{2j} \\ \tau_{3j} \end{Bmatrix}.$$

Here (x,y,z) are the Cartesian coordinates, (u ,v ,w) are the velocity components, ρ is the density, and p is the pressure. E is the total energy given by

$$E = e + \frac{u^2 + v^2 + w^2}{2},$$

$$e = c_v T, \quad p = \rho RT.$$

Here e is the internal energy and T is the temperature. The shear stress and the heat flux are given by

$$\tau_{ij} = \mu\left\{\frac{\partial u_i}{\partial x_j} + \frac{\partial u_j}{\partial x_i} - \frac{2}{3}\delta_{ij}\frac{\partial u_k}{\partial x_k}\right\}, \quad q_j = -k\frac{\partial T}{\partial x_j}.$$

The viscosity (μ) is computed using Sutherland's law and the coefficient of conductivity (k) is given in terms of the Prandtl number Pr. The variables ρ, p, T and velocity are non-dimensionalised by their corresponding reference variables ρ_∞, p_∞, T_∞ and $\sqrt{RT_\infty}$ respectively. The reference value for length is computed by $\sqrt{\nu x_0 / U_\infty}$, where x_0 is the location of the beginning of the computational domain from the leading edge in the streamwise direction. For the computation, the equations are transformed from physical coordinate system (x, y, z) to the computational curvilinear coordinate system (ξ,η,ζ) in a conservative manner and the governing equations become

$$\frac{\partial}{\partial t}\overline{Q}_i + \frac{\partial}{\partial x_j}\left(\overline{F}_{ji} - \overline{F}_{vji}\right) = 0.$$

The components of the flux in the computational domain are related to the flux in the Cartesian domain by

$$\overline{Q}_i = \frac{Q_i}{J}, \quad \left[\overline{F}_{ji}\right] = \frac{J}{|J|}\left[F_{ji}\right],$$

where $J = \left[\frac{\partial(\xi,\eta,\zeta)}{\partial(x,y,z)}\right]$.

Solution Algorithm

The governing equations are solved using the 5th-order accurate weighted essentially non-oscillatory (WENO) scheme for space discretization and using third-order total-variation-diminishing (TVD) Runge-Kutta scheme for time integration. The WENO and the TVD methods and the formulas are explained in Shu (1992) and the application of ENO method to N-S equations is given in Atkins (1991). The solution method used is described in an earlier paper Balakumar et. al. (2002).

The height distribution of a rough surface is generally determined using a Gaussian probability distribution and a correlation length (Saillard and Sentenac 2001). Before a general rough surface is considered, in this paper the disturbances induced by isolated roughness are studied. The roughness is assumed to be of Gaussian shape in the form

$$y = f(x,z) = he^{-\sigma_1(x-x_0)^2 - \sigma_2 z^2},$$

where h is the height of the roughness, σ_1 and σ_2 determine the width of the roughness in the streamwise and spanwise directions and $x=x_0$ is the location of the roughness. The grid is generated by transforming the surface into a straight line using the expression

$$\eta = \frac{y - f(x,z)}{H(x) - f(x,z)},$$

where y = H(x) is the outer boundary in the computational domain.

The acoustic field that impinges on the outer boundary is taken to be in the following form.

$$p' = \mathrm{Re}\,al\left\{\tilde{p}e^{i\alpha_{ac}x+i\beta z+i\varepsilon_{ac}y-i\omega t}\right\}.$$

Here α_{ac}, β_{ac}, ε_{ac} are the acoustic wavenumber, and ω is the frequency of the acoustic disturbance.

Results

First the flow field induced by two and three-dimensional isolated Gaussian shaped roughness elements of different heights are computed. Secondly, the disturbances generated by the interaction of two-dimensional acoustic disturbances with a blunted flat plate with and without roughness are computed. The flow parameters are given in Table 1.

Table 1.

Flow parameters for the wind tunnel model.

Freestream Mach number M_∞ = 3.5

Freestream Reynolds number $Re_\infty = 12*10^6$/ft

Freestream density $\rho_\infty = 2.249*10^{-2}$ lbm/ft^3

Freestream pressure ρ_∞ = 187.74 lbf/ft^2

Freestream velocity U_∞ = 2145.89 ft/s

Freestream temperature T_∞ = 156.42 $^\circ$R

Free stream kinematic viscosity $\nu_\infty = 1.7882*10^{-4}$ ft^2/s

Wall temperature = Adiabatic condition

Prandtl number Pr = 0.72

Ratio of specific heats γ = 1.4

Length scale $\sqrt{\frac{\nu_\infty x_0}{U_\infty}} = 5.892*10^{-5}$ *ft.*

(x_0 = 0.5 in.)

The boundary layer thickness at X=1 in. δ_0= .01275 in.

Non–dimensional frequency F = $1*10^{-5}$ = 41.0 kHz

The non-dimensional frequency F is defined as

$$F = \frac{2\pi\nu_\infty f}{U_\infty^2},$$

where f is the frequency in Hertz.

The grid is generated using analytical conformal mapping formulae. The grid is clustered in the η directions close to the wall and near the critical layer region and is also clustered in the ξ and ζ directions close to the roughness and is shown in figure 2. We present the results for the parameters x_0 =1 in., $\sigma_1 = \sigma_2$ = .25. here x_0 is the location of the roughness element from the leading edge.

Linear instability

As a prelude for future reference, in figure 3 the linear stability results for the boundary layer over a flat plate is presented. The figure depicts the neutral stability diagram in (Re, F), (Re,α) and (Re, β) planes for different wave angles 0, 45, 60 and 70 degrees. The figure also shows the N-Factor curves and the growth rates for the most amplified disturbances. The critical Reynolds number is about 193 and this occurs for an oblique wave of angle 60 degrees. The most amplified frequency is about F=1.0-1.25e-5 and the most amplified wave has a spanwise wavenumber of β=. 025 and this corresponds to about .178 inches in dimensional units and is equivalent to about 14 boundary layer thicknesses. It is also observed that at higher Reynolds numbers Re > 1000, only the low frequency disturbances F < 3.E-5 are unstable. This implies that acoustic disturbance with frequencies less than 120 kHz may be the relevant frequency range for generating instability waves inside the boundary layer. The frequency of the most amplified wave is about 40 kHz. The maximum N-factor at X=12 in, (Re = 3464) is about 8.6.

Steady flow due to the roughness.

In these computations, an isolated two and three-dimensional roughness are placed at X_0=1 in. from the leading edge. The Reynolds number at this location is $\sqrt{\frac{U_\infty x_0}{\nu_\infty}} = 1000.$ and the parameters in the Gaussian distribution $\sigma_1 = \sigma_2 = 0.25$. This gives the width of the roughness element as half the boundary layer thickness.

Two-dimensional roughness.

Figures 4-8 show the results for the two-dimensional roughness elements. The computations are performed for different roughness heights h/δ_0=1/16, 1/8, 1/4 and 1/2. Figure 4 shows the contours of density inside the boundary layer and in the inviscid region for two cases h/δ = 1/16 and 1/2. Steady solutions are obtained in all the cases and there is no vortex shedding observed. For h/δ = 1/2, in the inviscid region the results clearly show a compression wave in the front, an expansion wave in the middle and another compression wave at the end. As expected these waves are weaker for the small roughness h/δ=1/16 compared to h/δ=1/2. Figure 5 shows the contours of the normal velocity (V) and the streamline patterns inside the boundary layer near the roughness for roughness heights h/δ = 1/16, 1/8, 1/4 and 1/2. The interesting observation is the type of separation induced by the roughness. At small roughness heights h/δ=1/16 there is no separation observed and the flow goes over the roughness smoothly. For roughness heights 1/16 < h/δ < 1/4, flow separates downstream of the roughness. The flow separates slightly downstream of the peak of the roughness and for h/δ = 1/8 it reattaches at about 4 roughness heights downstream of the peak. For roughness heights h/δ > 1/4, the flow separates in the upstream and downstream of the roughness. The length of the separated regions increases with roughness height and for h/δ = 1/2, the upstream separated region is about 15h and the downstream region is about 8h.

Figure 6 shows the variation of the normal density in the streamwise direction (x) at constant heights y/δ_0 = 1 and 2 for different roughness heights h/δ_0 = 1/16, 1/8, 1/4, 1/2. As observed earlier, a smooth compression in the upstream, a sharp and a strong expansion fan across the roughness peak and a strong compression downstream are observed. The strength of these waves increases with increasing heights. In figures 7 and 8, the velocity profiles at different streamwise locations relative to the roughness location are presented and they are compared with the unperturbed Blasius velocity profiles. Figure 7 shows the difference between the velocity profiles induced by the roughness and the Blasius profiles at the upstream streamwise locations $(x-x_0)/\delta_0$ = -16, -4, -2 and at the downstream locations $(x-x_0)/\delta_0$ = 2, 4, 16. The first observation is that the modification to the boundary layer is more in the region upstream of the roughness than in the downstream of the region. The change in maximum velocity is about 1% at the upstream location $(x-x_0)/\delta_0$ = -2 and is about 0.3% at the downstream location $(x-x_0)/\delta_0$ = 2. The shape of the modification to the velocity profiles is also different from the upstream to the downstream. In the downstream, the velocity is reduced more near the wall and near the outer part of the boundary layer than in the middle of the boundary layer and this may have a strong influence in the stability characteristics. Figure 8 shows the velocity profiles and the comparison with the Blasius profiles for the roughness h/δ_0 = 1/2. Again the modification is larger in the upstream region of the roughness about 40% at $(x-x_0)/\delta_0$ = -4 compared to that in the downstream region which is about 15% at $(x-x_0)/\delta_0$ = 4. The difference from the Blasius profiles decreases with increasing distance from the roughness and it is less than 1% at $(x-x_0)/\delta_0$ = 20.

Three-dimensional roughness.

Figures 9 and 10 show the flow field induced by three-dimensional roughness of heights h/δ = 1/16 and 1/8. In the spanwise direction periodic boundary condition is applied. The wavenumber in the spanwise direction is β=.025, which

correspond to the most, amplified disturbance. Figure 9 shows the streamline patterns and the contours of the density in the (x-y) plane at z=0. In these cases also, steady solutions are obtained and no vortex shedding is observed. For the roughness height $h/\delta_0=1/8$ a small recirculation region is observed downstream. In the three-dimensional case the compression and the expansion waves are weaker compared to the two-dimensional case. Figure 10 shows the contours of the spanwise velocity component (w) in the (y-z) planes at different streamwise locations relative to the roughness location, $(x-x_0)/\delta_0$ =-2, 0., 7.5 and 190. for the roughness height $h/\delta_0=1/16$. Figures 10(a-c) show the flow field near the roughness height and the figure 10d shows the results far downstream from the roughness. The maximum spanwise velocity is about .02 and within about two boundary layer thicknesses upstream and ten boundary layer thicknesses downstream the velocities are reduced by two orders of magnitude. Figure 10d shows the flow field induced by the roughness in the inviscid part of the flow. Due to the periodic and symmetric boundary conditions at the boundaries the Mach waves radiated in the spanwise directions bounce back and forth inside the domain and this is clearly seen in figure 10d in the outer part of the flow field. This made the convergent to the steady state very slow.

Acoustic waves.

The linearized Euler equations in a uniform mean flow are:

$$\frac{\partial \rho}{\partial t}+U_0\frac{\partial \rho}{\partial x}+\rho_0\frac{\partial u}{\partial x}+\rho_0\frac{\partial v}{\partial y}+\rho_0\frac{\partial w}{\partial z}=0,$$

$$\rho_0\frac{\partial u}{\partial t}+\rho_0U_0\frac{\partial u}{\partial x}=-\frac{\partial p}{\partial x},$$

$$\rho_0\frac{\partial v}{\partial t}+\rho_0U_0\frac{\partial v}{\partial x}=-\frac{\partial p}{\partial y},$$

$$\rho_0\frac{\partial w}{\partial t}+\rho_0U_0\frac{\partial w}{\partial x}=-\frac{\partial p}{\partial z},$$

$$\rho_0c_p\frac{\partial T}{\partial t}+\rho_0U_0c_p\frac{\partial T}{\partial x}=\frac{\partial p}{\partial t}+U_0\frac{\partial p}{\partial x},$$

$$P_0=\rho_0RT_0,$$

$$p=\rho_0RT+\rho RT_0.$$

The solution of this system can be written as

$$\begin{Bmatrix}\rho\\ u\\ v\\ w\\ T\end{Bmatrix}=\begin{Bmatrix}\frac{1}{a_0^2}\\ -\frac{\alpha_{ac}}{\rho_0(\alpha_{ac}U_0-\omega)}\\ -\frac{\beta_{ac}}{\rho_0(\alpha_{ac}U_0-\omega)}\\ -\frac{\varepsilon_{ac}}{\rho_0(\alpha_{ac}U_0-\omega)}\\ \frac{(\gamma-1)T_0}{\rho_0a_0^2}\end{Bmatrix}p.$$

Here the pressure p is in the form

$$p=p_{amp}e^{i(\alpha_{ac}x+\beta_{ac}y+\varepsilon_{ac}z-\omega t)}.$$

The dispersion relation among the wavenumbers α_{ac}, β_{ac}, ε_{ac} and the frequency ω is given by

$$(\alpha_{ac}U_0-\omega)^2=(\alpha_{ac}{}^2+\beta_{ac}{}^2+\varepsilon_{ac}{}^2)a_0^2.$$

For zero sweep acoustic disturbances $\varepsilon_{ac}=0$, the wavenumber α_{ac} can be expressed as

$$\alpha_{ac}=\frac{\omega\cos\theta_y}{(U_0\cos\theta_y\pm a_0)}.$$

Here $\theta_y = \tan^{-1}\left(\frac{\beta_{ac}}{\alpha_{ac}}\right)$ is the incident angle and for $\beta_{ac} < 0$ the plate is radiated from above and for $\beta_{ac} > 0$ the plate is radiated from below or represents the wave which is reflected from the plate (figure 11). The plus sign corresponds to the fast moving wave and the minus sign corresponds to the slow moving wave. The corresponding phase speeds are $C = U_0 \pm \frac{a_0}{\cos\theta_y}$. The wavenumber of the fast moving wave is $\alpha_{ac} < \frac{\omega}{U_0 + a_0}$ and for the slow moving wave $\alpha_{ac} > \frac{\omega}{U_0 - a_0}$ and the incident angle is limited by $\theta_y < \cos^{-1}\left(\frac{1}{M}\right)$. At M=3.5, F=1.25E-5 the wavenumbers of the fast moving and slow moving waves are $\alpha_{ac} < 0.00687$ and $\alpha_{ac} > 0.01237$ and the incidence angle of the slow moving wave is limited to 73.39 degrees. The wavenumber of the acoustic disturbances α_{ac} for different incident angle θ_y is given in Table 2 for two different spanwise wavenumbers ε_{ac}.

Table 2.

Values of α_{ac} for different inclination angle

θ_y	ε_{ac}=0.0	ε_{ac}=.025
0	.01237	.01757
5	.01239	.01758
10	.01245	.01762
20	.01270	.01780
30	.01319	.01816
40	.01409	.01886

The variation of the wavenumber $\alpha$with the Reynolds number $\sqrt{\frac{U_\infty X}{\nu_\infty}}$ for a two-dimensional β=0 and a three-dimensional β=0.025 instability waves are plotted in figure 12. The wavenumber for the two-dimensional wave decreases from .0124 at a Reynolds number of 220 to .0119 at a Reynolds number of 2000. For the three-dimensional disturbance it decreases from .01775 at a Reynolds number of 190 to .01285 at a Reynolds number of 2000. The Reynolds number at the neutral points is 820 and 610 respectively for the two and three-dimensional disturbances and they are also marked in figure 12. In this figure the range of the acoustic wavenumber α_{ac} for the two and three-dimensional acoustic waves are also depicted. It is seen that perfect matching in the wavenumbers occur at very low Reynolds number range where the disturbances are marginally stable. For the unit Reynolds number of $12*10^6$, Reynolds number of 200 is located at .04 inches from the leading edge of the plate. Hence there may be strong generation of instability waves in the nose region where the bluntness effects will be important. In the neutral and unstable region the acoustic and the instability wavenumbers do not match and some tuning must occur due to nonparallel effects of the boundary layer or due to some inhomogenities on the surface such as rough nesses. In this paper the interaction of the acoustic waves with the boundary layer with and without roughness in the neutral and unstable region is investigated.

Acoustic waves and the continuous spectrum

The unsteady flow field in a boundary layer consists of all the discrete eigensolutions and the continuous spectrum, which appears because the domain is unbounded and the linearized stability equations admit solutions that are bounded at infinity. The details about the derivation and the computation of the discrete and the continuous spectrum are given in Balakumar and Malik (1992). For a supersonic boundary layer, there exist seven branches of the continuous spectrum in the complex wavenumber space. Two of them are the fast and slow moving acoustic waves. Hence the free-stream acoustic disturbances enter the boundary layer through the continuous spectrum.

The solution of the linearized stability equations in the free stream can be written as

$$\phi = \sum_{i=1}^{8} C_i q_i e^{r_i y},$$

where q_i (i=1,8) are column vectors and

$$r_1 = -\mu_1,\ r_2 = -\mu_2,\ r_3 = -\mu_3,\ r_4 = -\mu_4,$$
$$r_{51} = \mu_1,\ r_6 = \mu_2,\ r_7 = \mu_3,\ r_8 = \mu_4,$$
$$\mu_1 = \lambda_1^{\pm},\ \mu_2 = \lambda_2^{\pm},\ \mu_3 = \lambda_3^{\pm},\ \mu_4 = \lambda_4^{\pm},$$
$$\lambda_1 = \lambda_2 = i(\varepsilon - \omega)\,\mathrm{Re} + \alpha^2 + \beta^2,$$
$$\lambda_3 = \frac{1}{2}\left[b_{22} + b_{23} + \left[(b_{22} + b_{33})^2 + 4(b_{23}b_{32} - b_{22}b_{33})\right]^{\frac{1}{2}}\right],$$
$$\lambda_4 = \frac{1}{2}\left[b_{22} + b_{23} - \left[(b_{22} + b_{33})^2 + 4(b_{23}b_{32} - b_{22}b_{33})\right]^{\frac{1}{2}}\right],$$

$$b_{22} = \alpha^2 + \beta^2 - \mathrm{Re}(\alpha - \omega)^2 \frac{\left[\frac{3}{4}\gamma M^2 - (\gamma - 1)\Pr M^2\right]}{\frac{3}{4}\mathrm{Re} + i(\alpha - \omega)\gamma M^2},$$

$$b_{23} = \frac{\mathrm{Re}(\alpha - \omega)^2\left\{\frac{3}{4} - \Pr\right\}}{\frac{3}{4}\mathrm{Re} + i(\alpha - \omega)\gamma M^2},$$

$$b_{32} = -i(\alpha - \omega)(\gamma - 1)\Pr M^2\,\mathrm{Re},$$
$$b_{33} = i(\alpha - \omega)\Pr\,\mathrm{Re} + \alpha^2 + \beta^2.$$

The continuous spectrum in the α-plane are determined by solving these equations with

$$\lambda_1 = -\lambda_{10},\ \lambda_3 = -\lambda_{30},\ \lambda_4 = -\lambda_{40},$$

where $0 \le \lambda_{10}, \lambda_{30}, \lambda_{40} \le \infty$. The continuous spectrum correspond to acoustic waves are obtained from

$$\lambda_4 = -\lambda_{40} = -\mu^2.$$

In the limit of large Reynolds number this equation takes the form

$$-\mu^2 = \alpha^2 + \beta^2 - (\alpha - \omega)^2 M^2.$$

This is same as the dispersion relation for the acoustic waves and the inviscid continuous spectrum for a two-dimensional disturbance β=0 is given by

$$\alpha = \frac{\omega}{1 \pm \frac{1}{M\cos\theta_y}}.$$

The eigenfunction corresponding to the continuous spectrum is obtained by solving the linearized stability equations with an inhomogeneous boundary condition at the far field. Keeping only the bounded solution at the far field and discarding the exponentially growing solution, the solution in the far field corresponding to the acoustic wave continuous spectrum takes the form

$$\begin{Bmatrix} u \\ v \\ w \\ T \\ p \\ u' \\ w' \\ T' \end{Bmatrix} = C_1 q_1 e^{-\mu_1 y} + C_2 q_2 e^{-\mu_2 y} + C_3 q_3 e^{-\mu_3 y} + C_4 q_4 e^{-i\mu y} + C_5 q_5 e^{+i\mu y}$$

The first three terms in the right hand side represent the exponentially decaying solution and the last two terms represent the oscillatory acoustic disturbances. Between the last two terms, the first term is the incident acoustic wave and the second term is the reflected acoustic wave. Hence by fixing the amplitude of the incident wave, for instance the amplitude of the pressure of the incoming wave is selected as $C_4 q_{45} = p_0$, the coefficient C_4 can be fixed. Since there are eight equations with four unknowns C_1, C_2, C_3 and C_5, eliminating C_1, C_2, C_3 and C_5 the necessary four inhomogeneous

boundary conditions at the far field are obtained. After the eigenfunction is solved for, the values of C_1, C_2, C_3 and C_5 can be calculated, especially the amplitude and the phase of the reflected acoustic wave C_5 can be inferred.

Figure 13 shows the amplitude of the coefficient of the reflected wave C_5 as a function of the incidence angle at different Reynolds numbers for a two-dimensional and three-dimensional acoustic wave. For a two-dimensional wave it is seen that at low Reynolds numbers the reflection coefficient is very large at small incident angles. It is about 27 at 3 degrees at a Reynolds number of 100 and it decreases with increasing Reynolds numbers. For three-dimensional acoustic disturbances the maximum reflection coefficient occurs at larger incident angles compared to the two dimensional case. In figure 14, the amplitude of the density fluctuations obtained by solving the inhomogeneous problem with the acoustic forcing at the free stream is presented. The results show the distribution for two incident angles 1.5 and 10 degrees at two axial locations 0.1 and 4.0 inches from the leading edge. The first observation is that with increasing Reynolds number the direct acoustic response is decreasing and the second is that at the larger incident angle of 10 deg. the disturbance inside the boundary layer is an order of magnitude larger than at the small incident angle of 1.5 deg. Since the low Reynolds numbers occur very close to the leading edge, the bluntness effect and the non-parallel effect will influence these results.

As it is discussed in the introduction, the instability waves are generated inside the boundary layer by the free-stream disturbances and the roughness on the surface. Since the acoustic disturbances have the wavelengths in the same range as the unstable disturbances, the acoustic disturbances itself may induce the instability waves by interacting with the growing boundary layer. Hence to investigate the effects of the acoustic and the roughness calculations are performed with and without the roughness elements.

Interaction of two-dimensional acoustic waves with a boundary layer.

The model consists of a semi-infinite flat plate with a blunt leading edge. The leading edge is modeled as a super ellipse of the form

$$\frac{(x-a)^4}{a^4}+\frac{y^2}{b^2}=1.$$

Here b is the thickness of the plate and in accordance with the experiment it is taken as .001 inches. The aspect ratio a/b is taken as 10 hence the blunt leading edge is joined with the straight portion of the plate at x=. 01 inch, which is at a Reynolds number of 100.

Figure 15 shows the meanflow density contours computed using the WENO code. Figure 14a shows the entire domain and figure 14b shows the flow field near the leading edge. The leading edge shock is located approximately at .0002 inches, which is 1/5 leading edge thicknesses upstream. Computations are also performed with an isolated two-dimensional roughness element. The roughness is located at x=1 in. (. ($\sqrt{\mathrm{Re}_x}=1000$) and the height of the roughness is h=δ/16. Figure 16 (a, b) show the density contours including the leading edge shock and the Mach wave originating from the roughness. The flow field near the roughness is same as that computed earlier. The density profiles at x=.01, .05, .1, .5, 1., 3. inches. ($\sqrt{\mathrm{Re}_x}$ =100, 224, 316, 707, 1000, 1732) in the similarity coordinates are plotted in figure 17a. In figure 17b, the same profiles are plotted in similarity coordinates. The Blasius similarity profile is also included for comparison. It is seen that very close to the leading edge, there exists a strong shock and the compression expands over the leading edge and becomes weaker away from the nose region. The boundary layer profiles slowly approach the similarity profiles and even at X=3 in., the outer part of the profiles did not merge with the similarity profile.

After the mean flow is computed two-dimensional acoustic disturbances are introduced at the outer boundaries. The

computations are performed at different incidence angles 0, 1.5, 10, and of 30 degrees and the non-dimensional frequency is F=1.25E-4. The amplitude of the acoustic wave is $p_{ac}/p_{\infty} = .001$.

Figures 18-21 show the results for the incident angle of 0 degrees with the roughness element. Figure 18a shows the contours of the density fluctuations in the whole computational domain and figure 18b depicts the results inside the boundary layer. Figure 19 shows the maximum density fluctuations along the X direction with and without the roughness. First observation is that the roughness did not introduce any difference in the generation of disturbances inside the boundary layer compared to that generated by the acoustic disturbances alone. Hence to the first order, the disturbances inside the boundary layer are due to the direct interaction of the acoustic disturbances with the boundary layer. In figure 20a, the distribution of the amplitude of disturbances obtained from the simulation is plotted at different axial locations x= .5, .1, 3. inches. ($\sqrt{\mathrm{Re}_x}$ = 707, 1000, 1732) are shown for zero incident angles. The eigenfunctions obtained from linear stability and from the continuous spectrum are also included for comparison. The question is whether the disturbances inside the boundary layers are the eigenmodes or the disturbances forced by the acoustic waves. The eigenfunctions distribution obtained from the linear stability results and from the continuous spectrum are similar in this region and further analysis is needed before any conclusion is made. An important observation is that the disturbances are generated very close to the leading edge region and after that they continues to grow. Figure 21 shows the maximum density fluctuations for different incident angles 0, 10 and 30 degrees. It is seen that the disturbances generated inside the boundary layer at 0 and 10 degrees do not depend on the direction of the acoustic wave. This may be due to the symmetry of the problem. The acoustic waves are coming from the top and the bottom sides of the plate and since the disturbances are generated near the leading edge of the plate, the incidence angle does not make any noticeable difference in the amplitude of the disturbances. The disturbances generated by the acoustic waves at 30 degrees incident angle initially follows the amplitude for the smaller incident angles and decreases downstream before it starts to grow again. In figure 20b , the eigenfunctions obtained from the simulation, linear stability and the continuous spectrum are plotted.

Discussion and Conclusions

The receptivity process induced by the interaction of acoustic disturbances at different incident angles over a blunted flat plate with and without an isolated roughness is numerically investigated.

The steady field induced by the two and three-dimensional roughness is computed. The flow field induced by two-dimensional roughness exhibits different characteristics depending on the roughness heights. A smooth compression exists in the front of the roughness, a sharp and strong expansion occurs above the peak of the roughness and a strong compression takes place at the back of the roughness. At small roughness heights the flow passes smoothly over the roughness, at moderate heights the flow separates downstream of the roughness and at larger roughness heights the flow separates upstream and downstream of the roughness. The velocity defects is larger upstream of the roughness than that in the downstream. As expected the flow field induced by the three-dimensional roughness is weaker compared to the two-dimensional roughness.

The interaction of the acoustic waves with a blunted flat plate investigation showed that the instability waves are generated very close to the leading edge. The amplitude of the disturbances generated is about five times of the free stream acoustic disturbances. It is also revealed that the small incident angle of the acoustic wave which are impinging the plate symmetrically from the above and below the plate does not make much difference in the amplitudes compared to that produced by a wave which is parallel to the plate. Computations have to be continued further

downstream and have to be performed with asymmetric acoustic disturbances to see the effects of incident angles in generating the unstable waves. It is also found that isolated roughness do not contribute much in generating unstable disturbances compared to that is generated by acoustic disturbances. Further computations have to be done with distributed roughness with different length scales to verify this conclusion.

References

Atkins, H. L., "High-Order ENO Methods for the Unsteady Compressible Navier-Stokes Equations," AIAA Paper 91-1557, 1991.

P.Balakumar , Malik, M. R., "Discrete modes and continuous spectra in supersonic boundary layers," J. Fluid Mechanics, Vol. 239, 1992, pp. 631-656.

P. Balakumar, Zhao, H, Atkins, H. L., "Stabilty of Hypersonic Boundary Layers Over a Compression Corner," AIAA Paper 2002-2848.

Chen, F. J., Malik, M. R., Beckwith, I. E., "Comparison of Boundary Layer transition on a Cone and Flat Plate at Mach 3.5," AIAA-88-0411, 1988.

Fedorov, A. V., and Khokhlov, A. P., " Excitation of Unstable Modes in a Supersonic Boundary Layer by Acoustic Waves," Fluid Dynamics, No. 9, pp. 456-467, 1991.

Gaponov, S. A., "Interaction between a supersonic boundary layer and acoustic disturbances," Fluid Dynamics, 6, 1977.

Gaponov, S. A. and Smorodsky, B. V., "Supersonic Boundary Layer Receptivity to Streamwise Acoustic Field," IUTAM Symposium,, Spinger-Verlag, 1999.

Gaponov, S. A., "Excitation of Instability Waves in the Supersonic Boundary Layer by Sound," IUTAM Symposium Potsdam, Springer-Verlag, 1993.

Herbert, T., "Parabolized stability equations," Annual Review of Fluid Mechanics, Vol. 29, 1997, pp. 245-283.

Mack, L. M., "Boundary Layer Stability Theory," JPL Report No. 900-277, Nov. 1969.

Mack, L. M., "On the application of linear stability theory and the problem of supersonic boundary-layer transition," AIAA J., 13, No. 3, 1975.

Saillard, M., and Sentenac, A., "Rigorous solutions for electromagnetic scattering from rough surfaces," Waves in Random Media, Vol. 11, 2001, R103-R137.

Shu, Chi-Wang, " Essentially Non-Oscillatory and Weighted Essentially N0n-Oscillatory Schemes for Hyperbolic Conservation Laws," NASA/CR-97-206253 and ICASE Report N0. 97-65

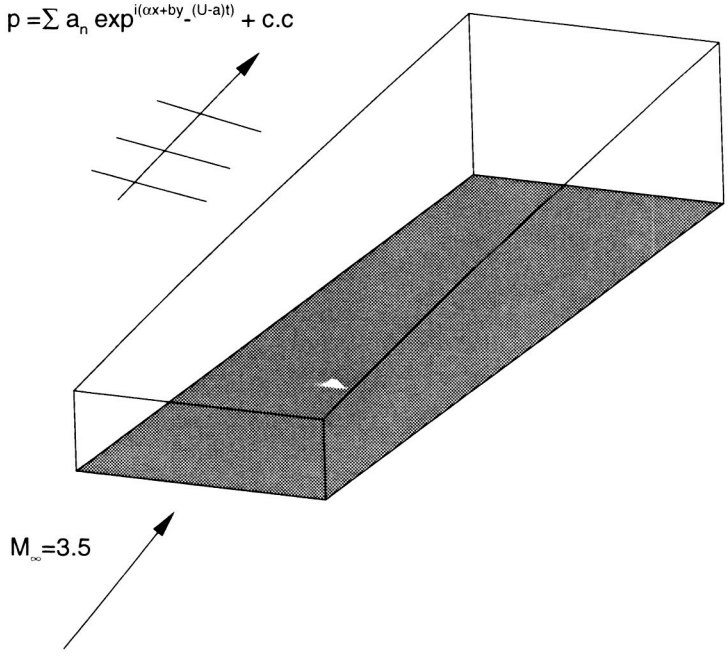

Figure 1. Schematic diagram of interaction of acoustic waves with roughness on the surface.

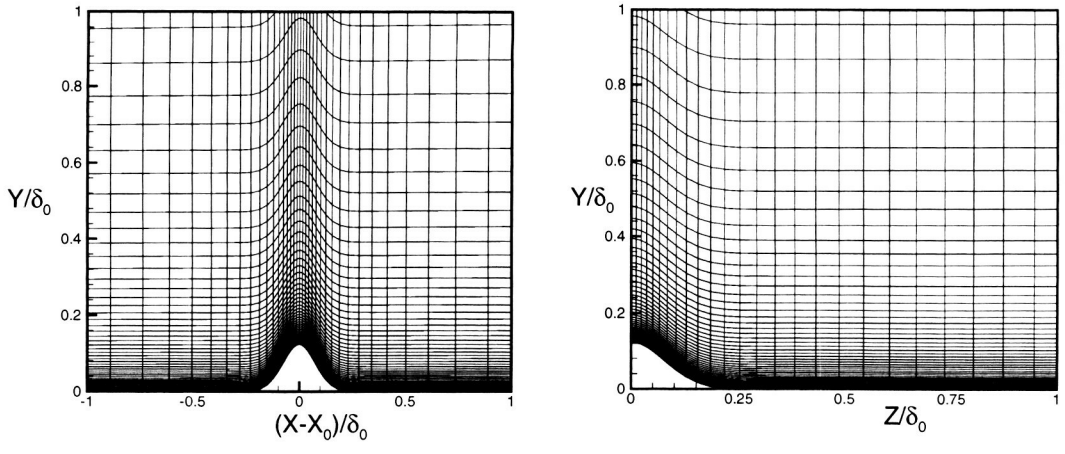

Figure 2. Grid distribution in the (x-y) and (z-y) planes.

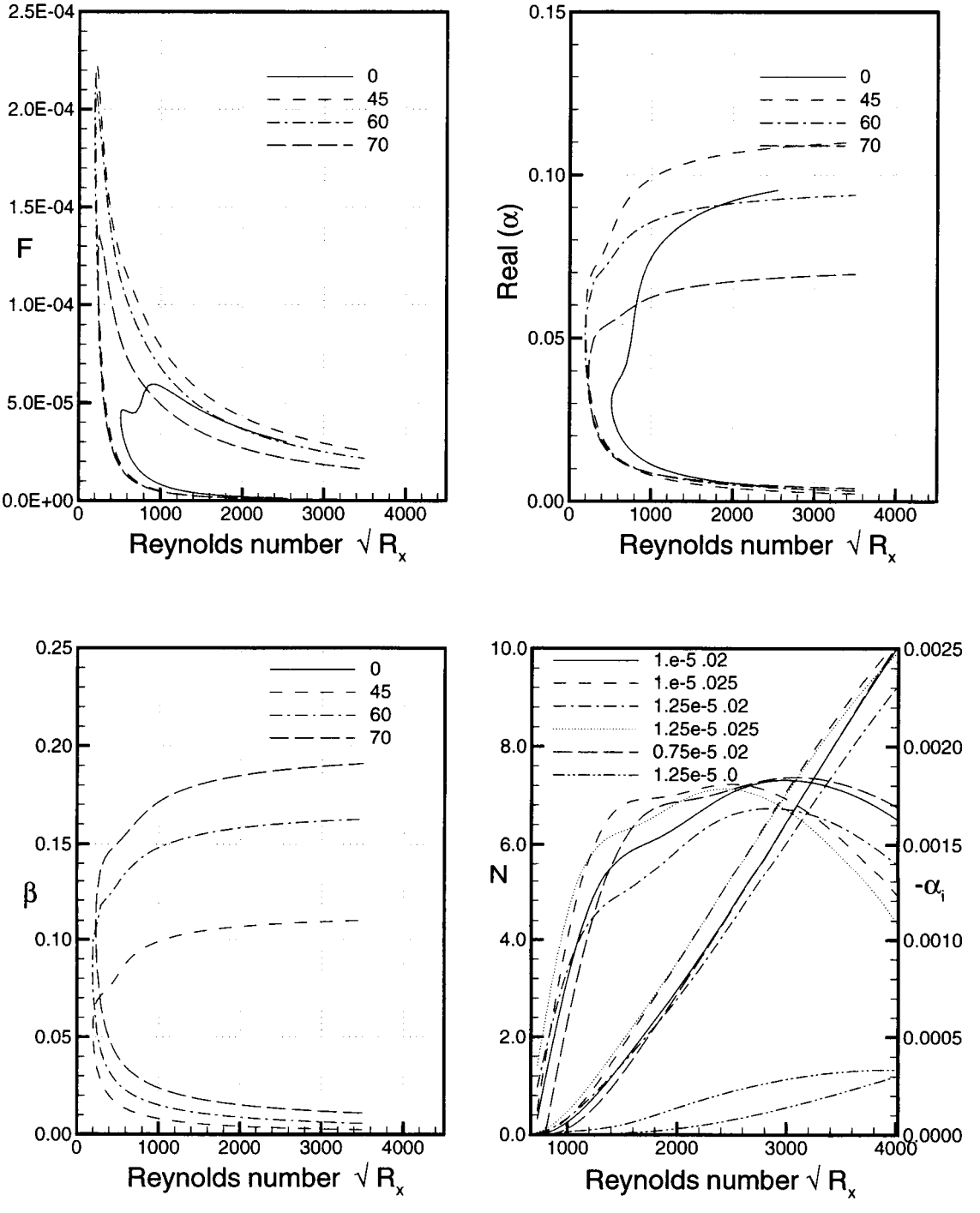

Figure 3. Stability and N-Factor digrams for a flat-plate boundary layer. $M_\infty = 3.5$ $T_\infty = 80°$ F.

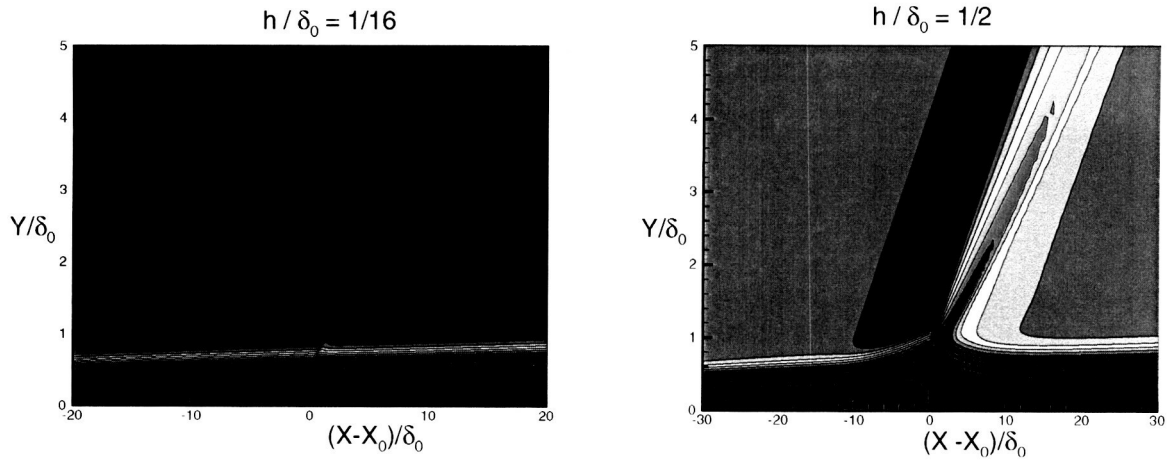

Figur 4. Contours of the density for flow over two-dimensional roughness elements of heights h/δ_0 = 1/16, 1/2.

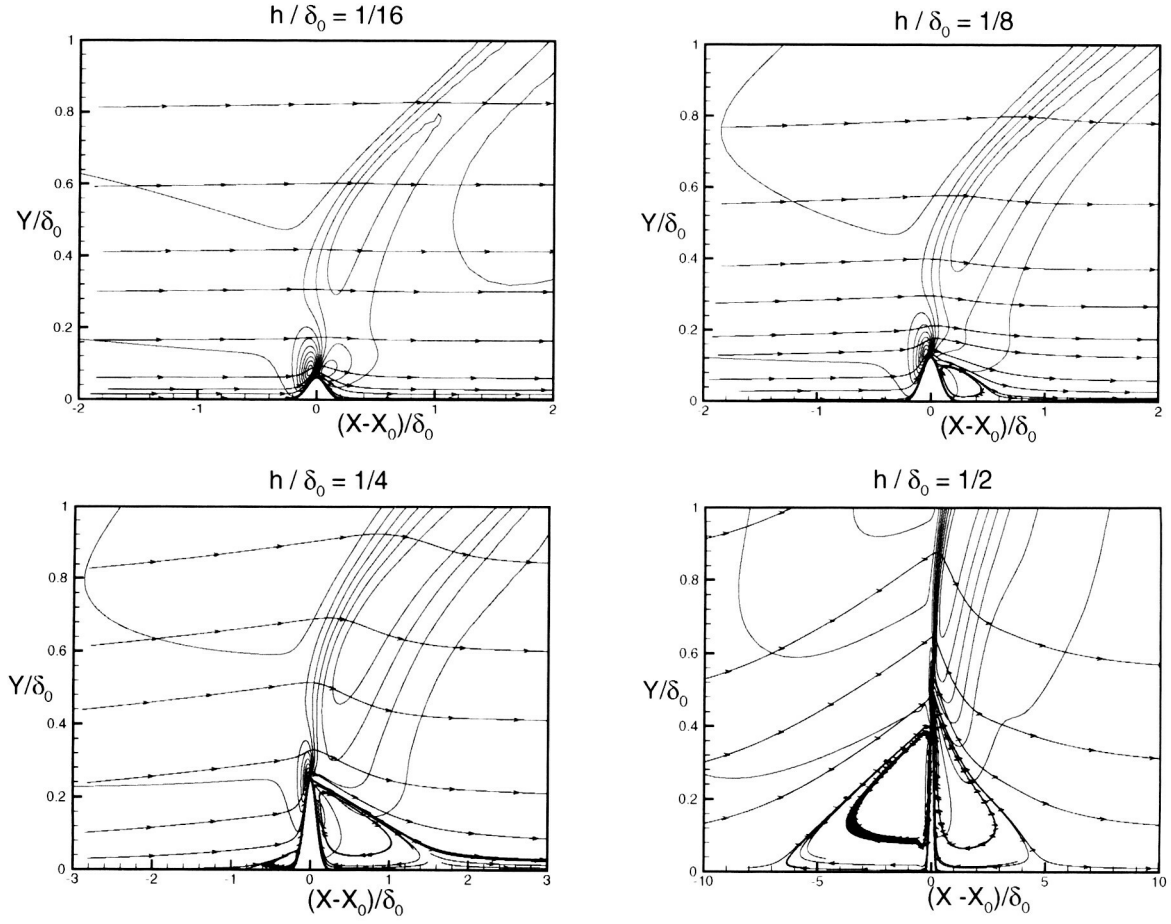

Figur 5. Contours of the normal velocity and the streamline patterns for flow over Gaussian two-dimensional roughness elements of heights h/δ = 1/16, 1/8, 1/4, 1/2.

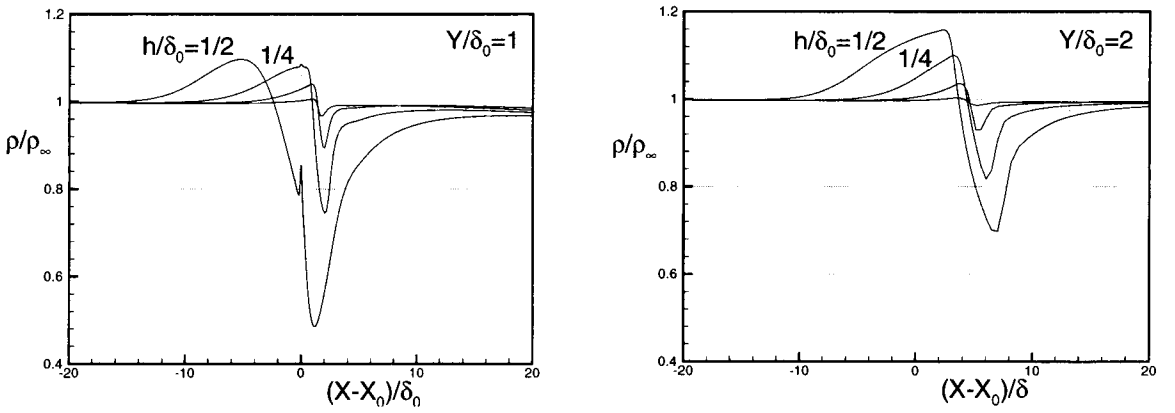

Figure 6. Variation of the density at constant heights $Y/\delta_0 = 1$ and 2 for different roughness heights $h/\delta_0 = 1/16, 1/8, 1/4, 1/2$.

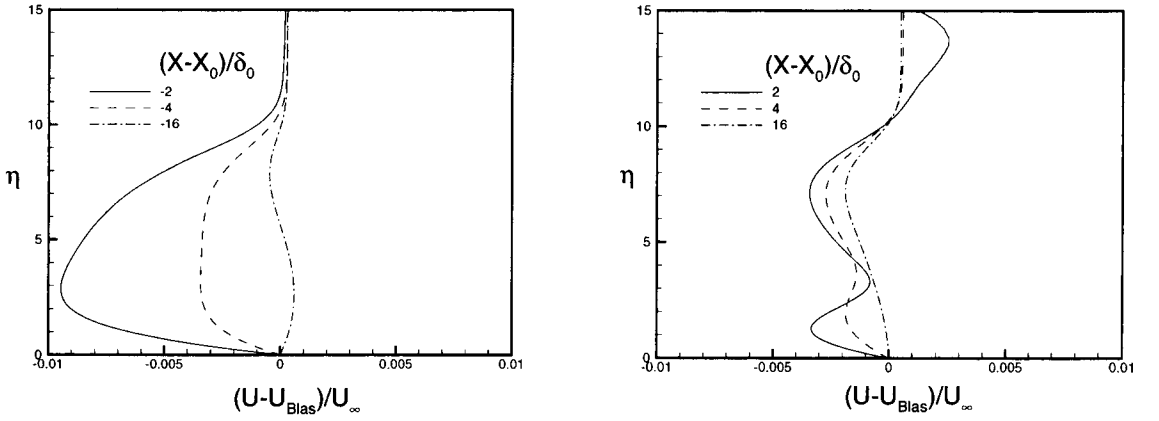

Figure 7. Modification to the U velocity profiles in the upstream and downstream locations due to the roughness elememt for roughness height $h/\delta_0 = 1/16$.

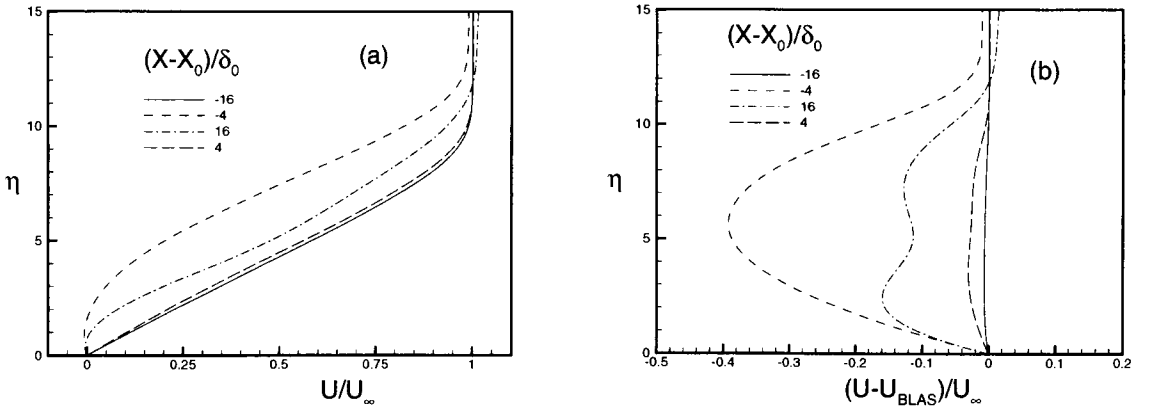

Figure 8. U velocity profiles (a) and the modification to the Blasius velocity profiles (b) in the upstream and downstream locations due to the roughness element of height $h/\delta_0 = 1/2$.

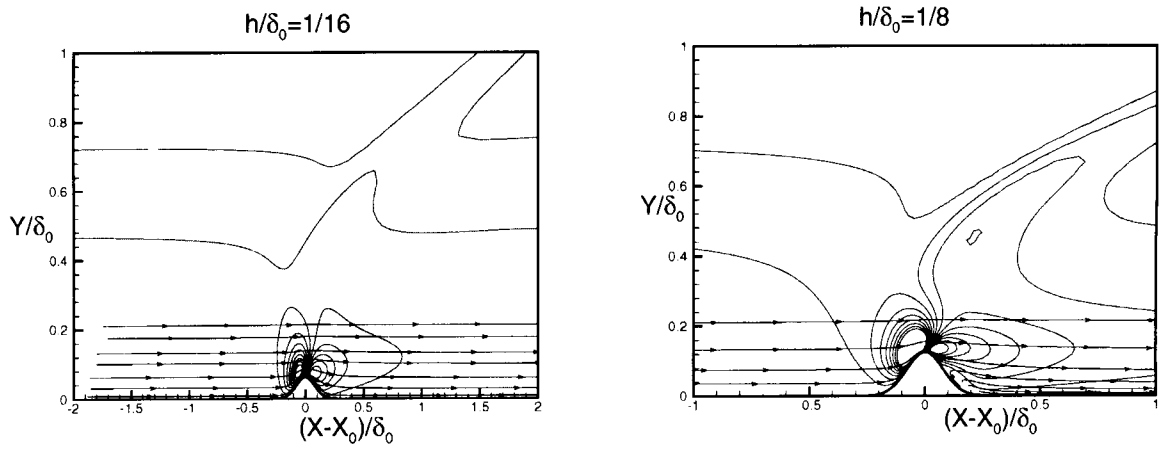

Figur 9. Contours of the normal velocity (V) and the streamline patterns for flow over Gaussian three-dimensional roughness elements of heights h/δ = 1/16, 1/8.

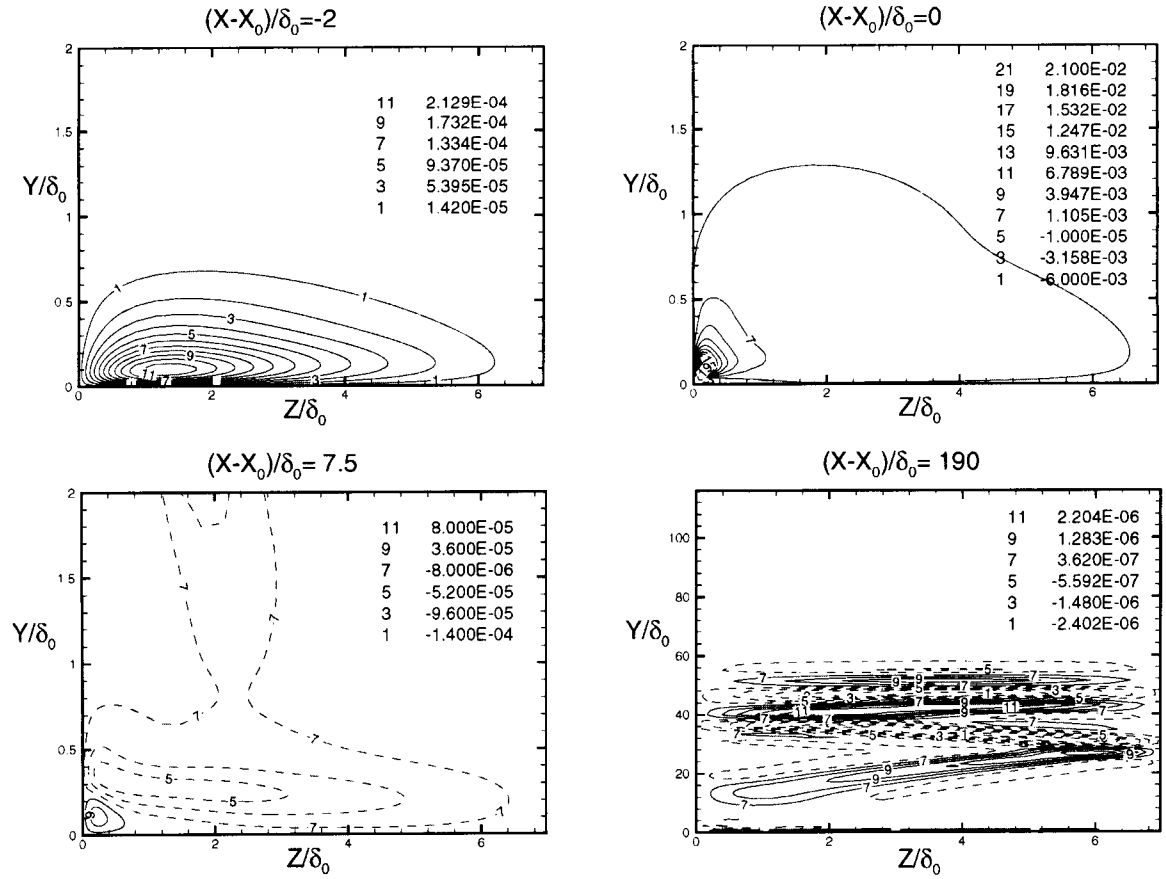

Figur 10. Contours of the spanwise velocity in the Z-Y plane at different sections $(X-X_0)/\delta$=-2, 0, 7.5, 190 for flow over a three-dimensional roughness element of height h/δ=1/16.

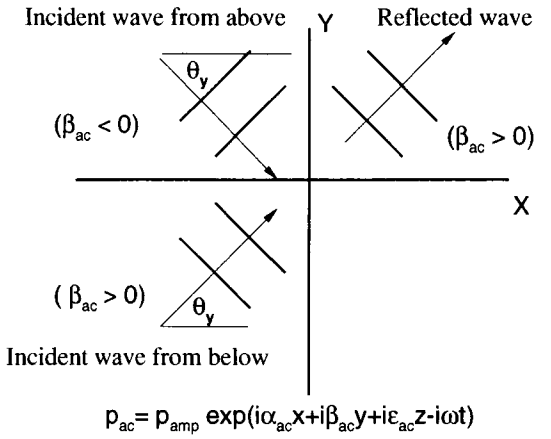

Figure 11. Schematic for the incident and the reflected acoustic field.

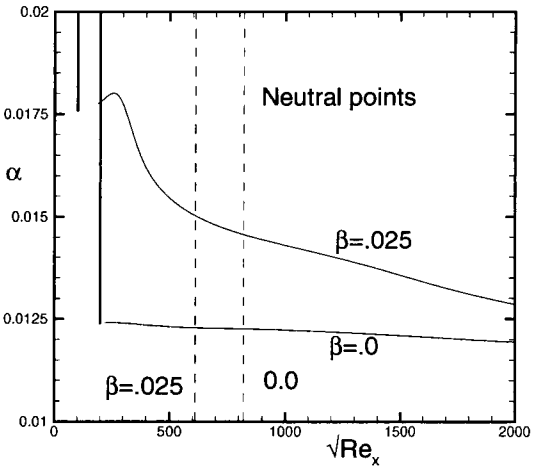

Figure 12. Variation of the wavenumber with the Reynolds number for the instability waves with β=0 and .025.

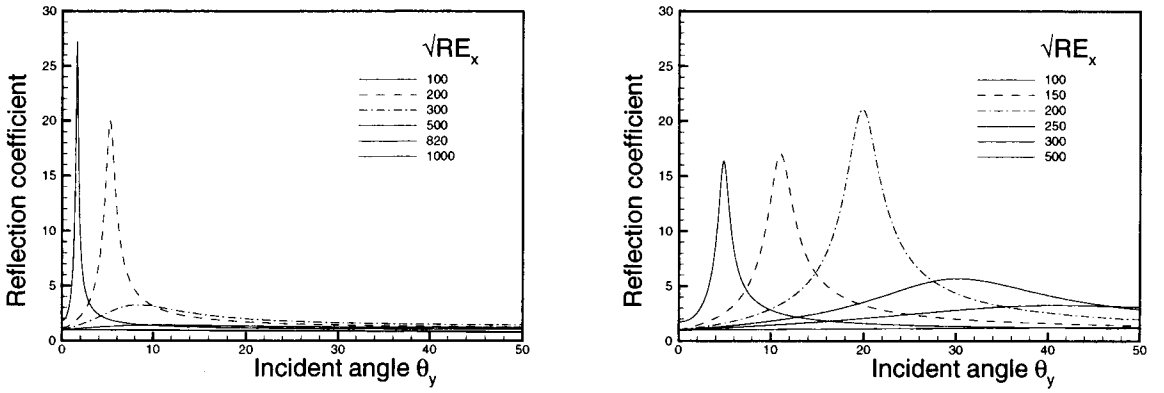

Figure 13. Variation of the reflection coefficient with the inclination angle at different Reynolds number for β=.0 and .025.

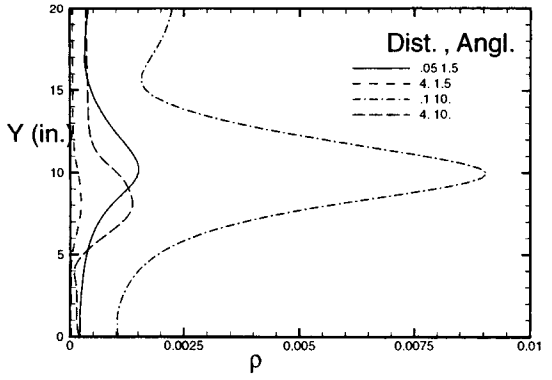

Figure 14. Density perturbations obtained by solving the continuous spectrum problem.

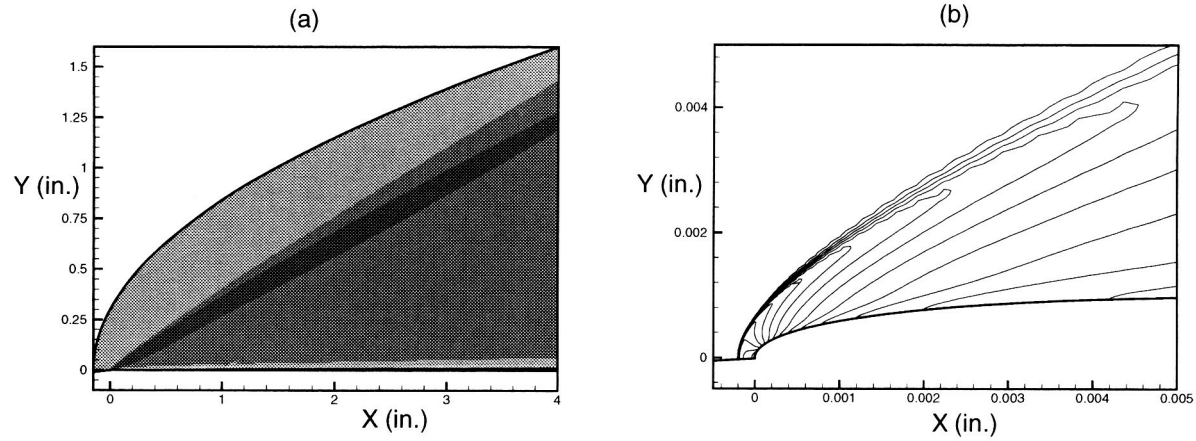

Figur 15. Contours of the density for flow over a flat plate with a blunted leading edge at M=3.5

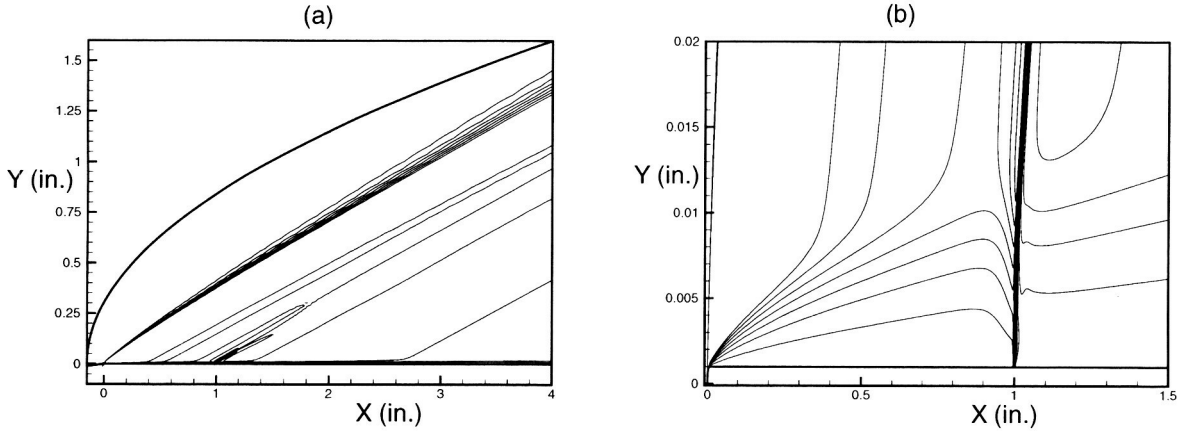

Figur 16. Contours of the normal velocity for flow over a flate plate with a blunted leading edge and an isolated roughness placed at X=1 in., M=3.5.

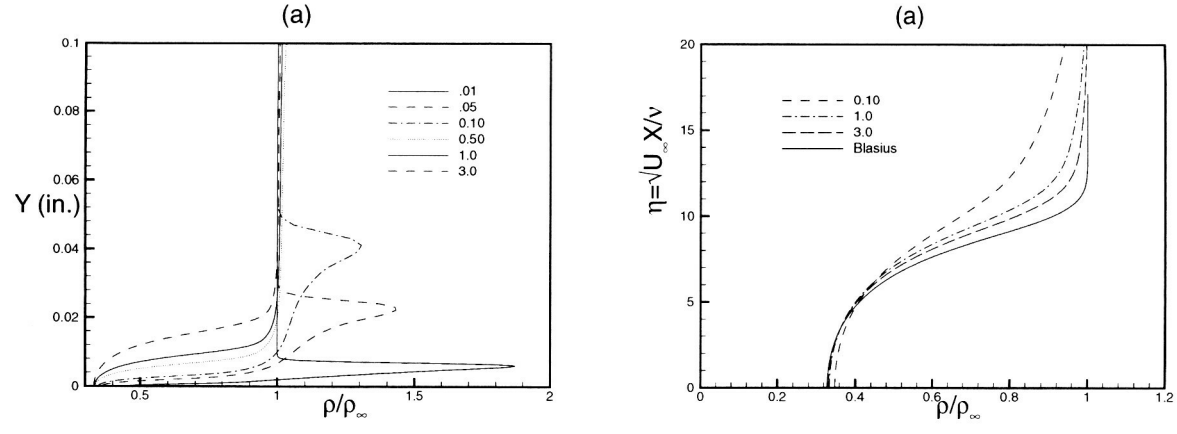

Figure 17. Mean density profiles at different X locations.

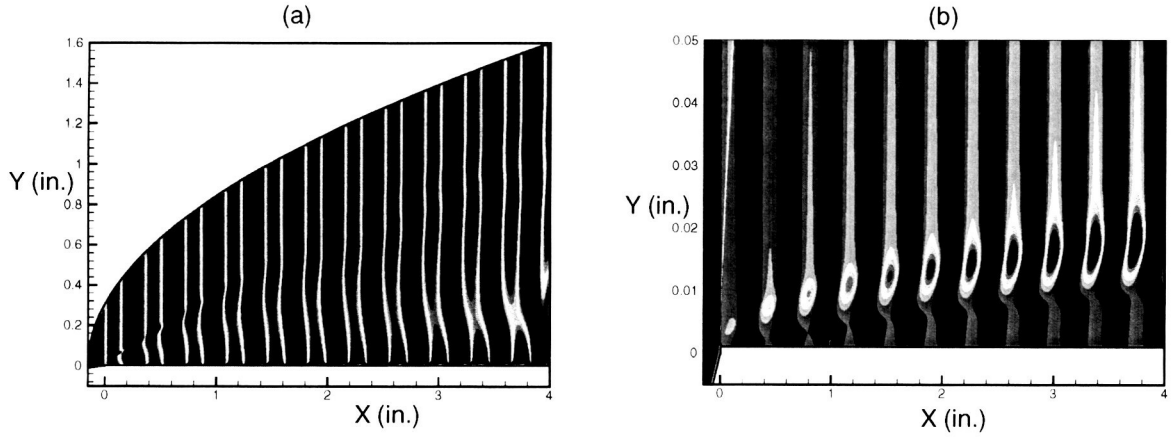

Figur 18. Contours of the unsteady density fluctuations due to the interaction of an acoustic wave with a flat plate with a blunted leading edge and a roughness. F=1.25E-4, incident angle 0.0 deg, M=3.5.

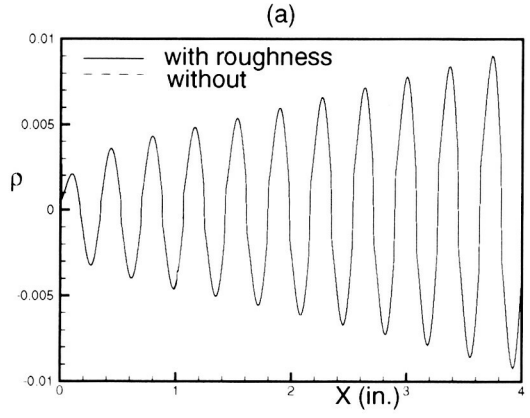

Figur 19. Maximum density fluctuation with and without roughness.F=1.25E-4, incident angle 0.0deg.

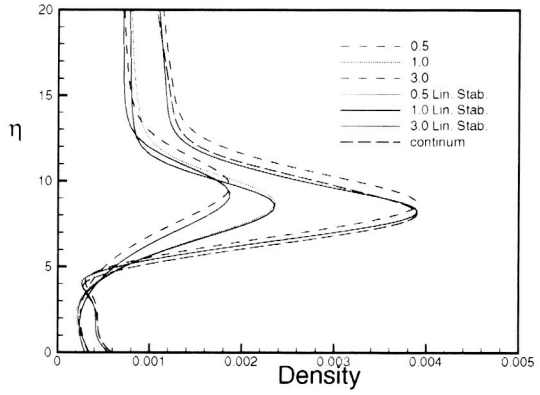

Figure 20a. Eigenfunctions obtained from simulation and linear stability at X=.5, 1., 3 inches. 0 deg.

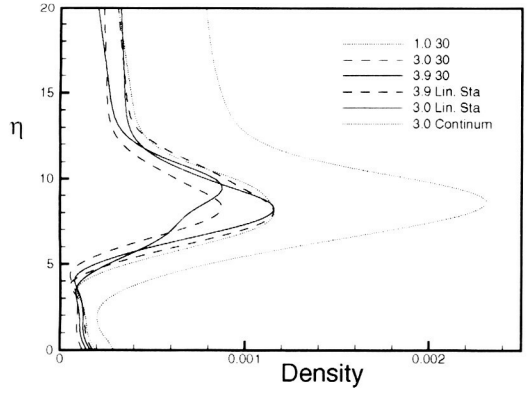

Figure 20b. Eigenfunctions obtained from simulation and linear stability at X= 1., 3 , 3.9 inches. 30 deg.

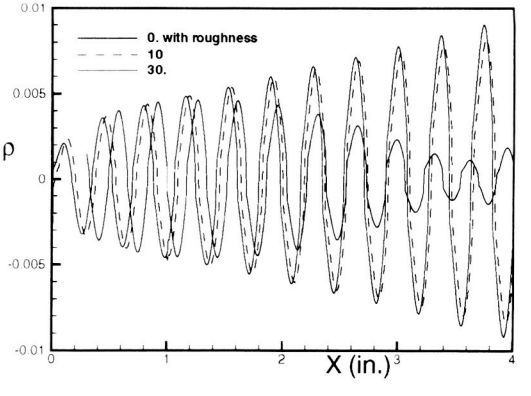

Figure 21. Maximum density fluctuations at different incident angles 0, 10 and 30 degrees.